Molecular Crystals and Liquid Crystals
Publication details, including instructions for authors and subscription information:
http://www.tandfonline.com/loi/gmcl16

The Temperature Dependence of the Dielectric and Conductivity Anisotropies of Several Liquid Crystalline Materials

R. T. Klingbiel [a] , D. J. Genova [a] & H. K. Bücher [a]
[a] Research Laboratories, Eastman Kodak Company, Rochester, New York, 14650
Version of record first published: 21 Mar 2007.

To cite this article: R. T. Klingbiel , D. J. Genova & H. K. Bücher (1974): The Temperature Dependence of the Dielectric and Conductivity Anisotropies of Several Liquid Crystalline Materials, Molecular Crystals and Liquid Crystals, 27:1-2, 1-21

To link to this article: http://dx.doi.org/10.1080/15421407408083116

Mol. Cryst. Liq. Cryst., Vol. 27, pp. 1–21

Printed in Dordrecht, Holland

The Temperature Dependence of the Dielectric and Conductivity Anisotropies of Several Liquid Crystalline Materials

R. T. KLINGBIEL, D. J. GENOVA and H. K. BÜCHER

Research Laboratoties
Eastman Kodak Company
Rochester, New York 14650

(Received January 30, 1973)

The temperature dependence of the conductivity and dielectric anisotropies are reported for several liquid crystalline materials of varying structure. The types of compounds studied are Schiff bases, *p*-phenyl benzoates, and phenyl-*p*-benzoyloxy benzoates, having either carbonate or alkyl terminal substituents. The anisotropies are computed from the bulk conductance and capacitance measured both parallel and perpendicular to an external magnetic field. The sign and magnitude of the anistropies are sensitive to changes in molecular structure as well as to phase transitions among the mesophases. Changes in sign of the conductivity anisotropy, dielectric anisotropy, or both, were found to occur with changing temperature in the alkoxy-carbonate Schiff bases, whereas no such anomaly was observed for the carbonate-alkoxy homologs. In such anisotropy sign reversals, there occurs a depression in $\epsilon_{\parallel}$ which is frequency-independent from 10-10^5 Hz. A sign reversal in the dielectric anisotropy also occurs in the phenyl-*p*-benzoyloxy benzonates, because of an unusually low frequency dielectric loss in $\epsilon_{\parallel}$. The loss appears to occur as a single relaxation process with a characteristic frequency of 10 kHz at about 50°C. The dielectric behavior of the *p*-phenyl benzoates shows a nearly constant anisotropy throughout their nematic range.

INTRODUCTION

One of the most interesting characteristics of liquid crystals is their ability to interact with external electric fields in such a manner as to permit a macroscopic reordering of the fluid. The body torques arising in the fluid upon application of an electric field may occur as a result of the anisotropy of the dielectric permittivity or, as shown by Carr[1] and Helfrich,[2] from shear-induced torques arising from the conductivity anisotropy. Many practical applications rely upon these electric-field-induced rearrangements and consequently there exists an interest in knowing how these anisotropies vary with liquid crystal composition. In our effort to contribute to the development of new liquid crystalline materials, having the optimum electrical and thermal properties for various specialized applications, we have examined the dielectric and conductivity anisotropies of many new materials. We report here a few examples representative of several types of compounds of recent interest to us.

EXPERIMENTAL PROCEDURE

Our experimental procedure is, basically, to orient a liquid crystal by means of an external magnetic field and then measure the sample capacitance and conductance both parallel and perpendicular to that magnetic as a function of temperature. The dielectric permittivity, ϵ, and conductivity, σ, calculated from these measurements are then labeled $\epsilon_\parallel$, $\epsilon_\perp$ or $\sigma_\parallel$, $\sigma_\perp$ for the electric field parallel or perpendicular to the magnetic field, respectively. We shall also speak of the isotropic averages $\epsilon = (\epsilon_\parallel + 2\epsilon_\perp)/3$ and $\sigma = (\sigma_\parallel + 2\sigma_\perp)/3$ as well as the anisotropies $\Delta\epsilon = (\epsilon_\parallel - \epsilon_\perp)$ and $\Delta\sigma = (\sigma_\parallel - \sigma_\perp)$. It is seen that the anisotropies may be positive or negative depending on the relative magnitudes of their parallel and perpendicular contributions. The effectiveness of the magnetic field to align the material depends on the temperature (and therefore the degree of order in a particular mesophase), the influence of the container walls, the magnetic field intensity, and the material's diamagnetic susceptibility anisotropy. For the compounds studied to date, a ten-kilogauss magnetic field appears adequate to align the director parallel to the magnetic field for the nematic phase, but is inadequate to dominate orientation in the smectic phases. We shall say more on this point later.

Assume, for the present, that we are concerned only with the nematic phase. It is well known[3] that below a critical value of the magnetic field, H_c, there is no reorientation; at high magnetic fields there is a saturation as the material reorients throughout the entire sample container. At fields such that $H/H_c \sim 20$, $\sigma/\sigma_\parallel$ approches 98 percent of $\sigma_\perp/\sigma_\parallel$ and corresponds to a nearly perfect perpendicular orientation throughout the sample thickness. We can acquire

such high H/H_c values by keeping H_c low. Since[3,4] $H_c^2 = \pi K_{ii}/\Delta\chi$ [where K_{ii} is a Frank[4] curvature elestic constant, $\Delta\chi = (\chi_\parallel - \chi_\perp)$ is the diamagnetic susceptibility anisotropy (both constants of the material), and d is the cell thickness], we decrease H_c by going to "thick" cells. For nematic materials typically $H_c \cdot d = 50\,kG \cdot \mu m$; in this work we therefore used $125 \cdot \mu m$ spacers for a 10kG field.

Since the conductivity anisotropy is dependent upon the ionic conducting species, the samples were first purified to as high a resistivity as possible; the resistivity was then substantially reduced by adding a high-purity quarternary ammonium salt, tetra-n-butylammonium perchlorate. Representative conductivities at room temperature would be 10^{-11} $(ohm\text{-}cm)^{-1}$, initially, and then would be reduced to $\sim 10^{-9}$ $(ohm\text{-}cm)^{-1}$ (approximately 1×10^{-4} mole percent salt). The AC potential applied to measure ϵ and σ is below any known threshold voltage associated with electric-field-induced instabilities. The liquid crystalline samples were filled into the cell as isotropic liquids and the sample was cooled at approximately 1°C/min with the magnetic field parallel to the electric field until the sample crystallized. The simultaneous measurement of $\sigma_\parallel$ and $\epsilon_\parallel$ constitutes a "cooling curve." It was then heated at the same rate and configuration to record a "heating curve." Finally, the sample was rotated 90° with respect to the magnetic field and a second cooling curve and heating curve were obtained for $\sigma_\perp$ and $\epsilon_\perp$. Any change in the conductivity of the isotropic phase is a sensitive measure of thermal decomposition of the material. No appreciable change in σ_{iso} was observed during the four temperature cycles.

CAPACITANCE AND CONDUCTANCE MEASUREMENT

The cell capacitance and conductance are measured simultaneously by means of two lock-in amplifiers. (See Figure 1.) A small amplitude sinusoidal voltage is applied to the cell and the out-of-phase current component, i_c, and the in-phase current component, i_r, are measured. The capacitance of the cell is directly proportional to i_c and the conductance of the material is directly proportional to i_r. A current-to-voltage conventer converts i_c and i_r to the respective voltages, v_c and v_r.

For the sake of convience, the observed capacitance and conductance of the liquid crystal is compared with that of a capacitor and resistor of known value. By measuring the capacitance of the empty cell, C_o, the cell geometry need not be known to calculate ϵ or σ. In either case, the cell geometry should be designed as to minimize the stray capacitance, C_p. A low C_p relative to C_o reduces the uncertainty in ϵ or σ.

In practice, the sample capacitance is usually measured at 10 kHz, to prevent v_r from exceeding the dynamic range of the signal amplifier section of the lock-in amplifier when v_r/v_c is large. This is necessary when either the liquid

crystalline materials are doped with ionic species or have a high concentration of ionic contaminants. As the phase angle, $\theta = \arctan(i_c/i_r)$, becomes smaller, say below 30°, drift in the phase angle stability of the lock-in amplifier increases the relative error in ϵ even though i_r is carefully phased out. Rapid changes in the conductance of the liquid crystal with temperature, especially near a phase transition, can introduce an error in ϵ when θ is low.

For materials that show a low frequency dielectric loss, it may be necessary to make dielectric measurements at 100 Hz or less. This is not a problem with materials that are purified to a resistivity $\gtrsim 10^9$ ohm-cm.

For conductance measurements, it is convenient to use low frequencies to prevent a relatively large v_c from exceeding the dynamic range of the signal amplifier section of the lock-in amplifier when v_c/v_r is large. This applies especially to liquid crystalline materials with a high resistivity. Low frequency conductance measurements approximate the direct current conductance of the material without the inherent difficulties of direct current measurements such as electrolysis, electrode polarization, and base line drift. At frequencies below 10 Hz, it becomes more difficult to filter out the alternating component of the lock-in amplifier output to the recorder in order to obtain the conductance as a smooth function of temperature.

The capacitance and conductance of the liquid crystalline material are measured simultaneously as a function of temperature at a frequency optimum to each. This is accomplished with two Princeton Applied Research Corporation (PAR) model 220 lock-in amplifiers as shown in Figure 1. The reference signal from one lock-in amplifier is applied to the noninverting input of an instrumentation amplifier while using the inverting input for the second lock-in amplifier. This allows the reference signal amplitude of each lock-in amplifier to be adjusted independently. The instrumentation amplifier has a large dynamic range which allows the two reference frequencies to be power amplified to a very low output inpedence without intermodulation distortion. The low impedence output prevents the cable and the cell capacitance from attenuating high frequency reference signals. This minimizes an additional phase shift due to the capacitive load which can vary as the dielectric constant changes with temperature.

The frequency range of the PAR model 220 is from 1 Hz to 110 kHz. The voltage to the cell never exceeds 1.0 volts peak to peak.

The output voltage from the instrumentation amplifier is applied either to the cell or to a parallel capacitor and resistor of known values. The current flowing through either the cell or parallel resistor and capacitor is converted to voltage by means of an operational amplifier with 10^{11} ohm input impedence, wide bandwidth, and large dynamic range. The output voltage is applied to an attenuator preceding the signal input amplifier of each lock-in amplifier in order to match the input voltage requirements (10 millivolts maximum).

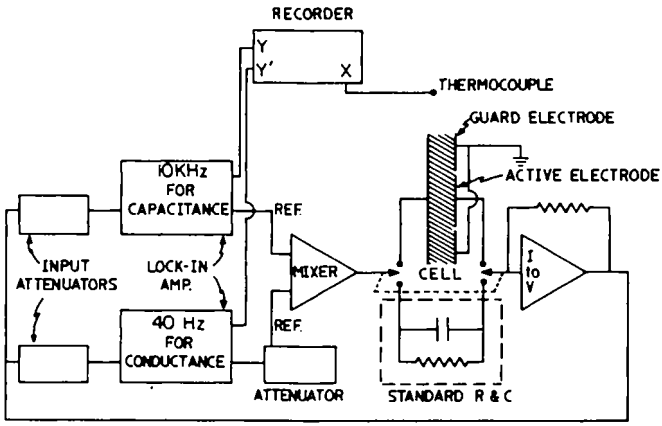

FIGURE 1 Schematic representation of the experimental procedure for measuring sample capacitance and conductance.

Normally the range of i_c for most liquid crystalline materials is less than fivefold. However, the range of i_r for a material with a wide mesomorphic range may be several orders of magnitude. To obtain precise conductivity data over a broad range, the attenuation of the reference signal to the instrumentation amplifier input is decreased stepwise toward unity as the conductivity of the sample decreases. This prevents the dynamic range of the electronics from being exceeded at high conductivity while maintaining a good signal-to-noise ratio at very low conductivities.

The data are displayed on a x, y, y' recorder. The x channel is connected to a thermocouple, the y and y' channels are connected to the respective lock-in amplifiers for capacitance and conductance data.

Cell design

The electrodes of the cell are designed for minimum stray capacitance, C_p. The electrodes are of glass with a conducting layer of tin oxide or indium oxide on one surface (Nesa and Nesatron respectively from Pitssburgh Plate and Glass Company, Pittsburgh, Pa.). One electrode is connected to the reference signal source. On the second plate, the conductive coating is cut by a thin scratch so as to form an isolated active electrode surrounded by a guard electrode. The anti-fringing guard electrode is connected to ground. The active electrode area is connected to the input of the operational amplifier which is driven toward virtual ground by the feedback resitor, R_L. As a result, the electric field across the active electrode area remains uniform. Fringing will be at a minimum if the width of the scratched line is kept narrow.

Teflon spacers are used between the plates, since Teflon can withstand large temperature extremes without contaminating the sample or undergoing mechanical distortion. A cell holder was designed to provide uniform pressure to the electrodes. The cell holder is then mounted on a thermostated block which can be rotated through 360°. The complete cell assembly is placed between the pole pieces of the magnet.

The temperature of the sample is measured with a copper-constantan thermocouple centered on the outside surface of one electrode. Two-mil wire is used to minimize heat conduction away from the thermocouple junction. Heat-conducting grease on the thermocouple and the outer surface of the electrode assures thermal contact. To further minimize error in the temperature measurement, the whole cell assembly is jacketed to reduce heat loss through convection to the air.

Estimate of error

The dielectric constant is calculated from equation 1:

$$\epsilon = \frac{(C_s - C_p)}{(C_o - C_p)} \tag{1}$$

Where C_s is the observed capacitance of the sample, C_o is that of the empty cell, and C_p is the parasitic capacitance.

The specific volume conductivity is calculated from $\sigma = G\,(t/A)$, where G is the observed conductance, t the cell thickness and A the electrode cross sectional area. The quantity (A/t) is obtained indirectly from $(C_o - C_p) = 0.0855\,\epsilon_o\,(A/t)$. Where ϵ_o is the dielectric constant of air and is taken as unity. The capacitance is in picofarads. The last two expressions are combined to eliminate (t/A) to obtain equation 2.

$$\sigma = \frac{0.0885\,G}{(C_o - C_p)} \tag{2}$$

The units for σ are $ohm^{-1}-cm^{-1}$.

Since ϵ is calculate from equation 1, the absolute value of the capacitance need not be known to any great precision. However, C_p must be evaluated to assure the accuracy of ϵ. C_p arises from two main sources: (a) stray capacitance from the leads to the cell, the physical placement of the electronic components and the internal leakage, and (b) fringing along the perimeter of the electrodes. The contribution due to the former is 0.04 pf and to the fringing is 0.02 pf. The latter was estimated by comparing the observed dielectric constants of Eastman White Label toluene ($\epsilon = 2.394$), chlorobenzene ($\epsilon = 5.592$), ethyl acetate ($\epsilon = 5.982$), and 1,1-dichloroethane ($\epsilon = 10.36$) at 25°C with the literature values of these materials[1] which are 2.379, 5.621, 6.02, and 10.36, respectively.

Typical observed empty cell capacitances range from 12.5 pf to 15 pf.

Since the empty cell capacitance is used to calculate G in equation 2, an error is introduced by the uncertainty in the absolute value of C_0. This uncertainty is ±1 percent from the precision of the selected capacitors plus an estimated uncertainty of +0.5 percent from stray capacitance within the paralleled standard resistance and standard capacitance boxes. Using ±1.3 percent precision carbon film resistors, this could result in a maximum error in the conductance of −2.5 to +1.5 percent.

RESULTS

a. *Dielectric and Conductivity Anisotropy Reversals:* We shall begin discussing our results in terms of somewhat familiar data, not necessarily new to the literature. Figure 2 shows the conductivity and dielectric anisotropies of N-(*p*-methoxybenzylidene)-*p*-butylaniline (MBBA). We observe that the dielectric anisotropy is negative and the conductivity anisotropy positive. The Helfrich criterion[2] for "dynamic scattering"[5] requires opposite signs in the dielectric and conductivity anisotropies so that we recognize this material as potentially useful for "dynamic scattering." We observe also that the temperature dependence of

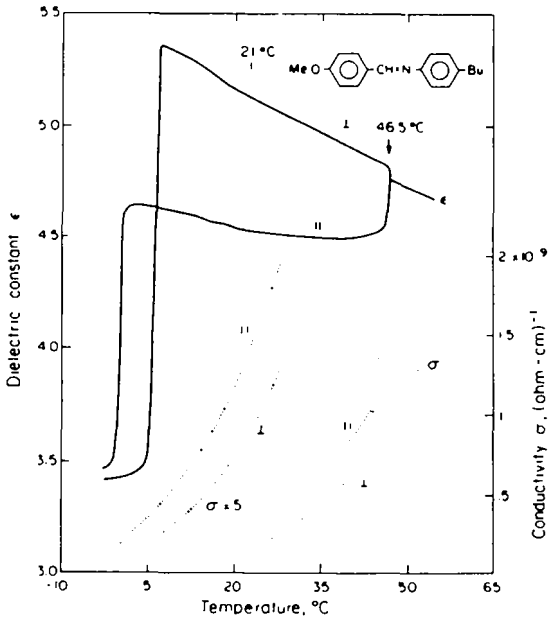

FIGURE 2 *Dielectric and conductivity anisotropy of MBBA.*

$\epsilon_\perp$ is nearly linear with a slight deviation near 19°C, but with the same slope upon supercooling to ~6°C, at which temperature it crystallizes. There is a larger variability in the temperature dependence of $\epsilon_\parallel$, especially near the clearing temperature, T_c. A slight deviation in $\epsilon_\parallel$ also occurs in the neighborhood of 19°C, which corresponds to the region of the melting temperature, represented by a vertical bar at 21°C. We note in addition that the conductivity does not reflect the deviations near 19°C. A deviation in the order parameter as determined by epr has been reported[7] to be in the same temperature region for MBBA.

Not all Schiff base data are so simply behaved, however. Figure 3 shows the anisotropies associated with N-(*p*-octyloxybenzylidene)-*p*'-octyloxycarbonyloxyaniline. This compound is isotropic above 95°C, as is evident from the disappearance of the dielectric and conductivity anisotropy. A nematic phase exist between 81° and 95°C, with two smectic phases appearing at lower temperatures: smectic I between 72.5 and 81°C, and smectic II below 72.5°C. The crystalline melting point is 60°C and therefore the crystallization upon cooling to 32°C represents a supercooling of the liquid by nearly 30°C. Notice that crystallization

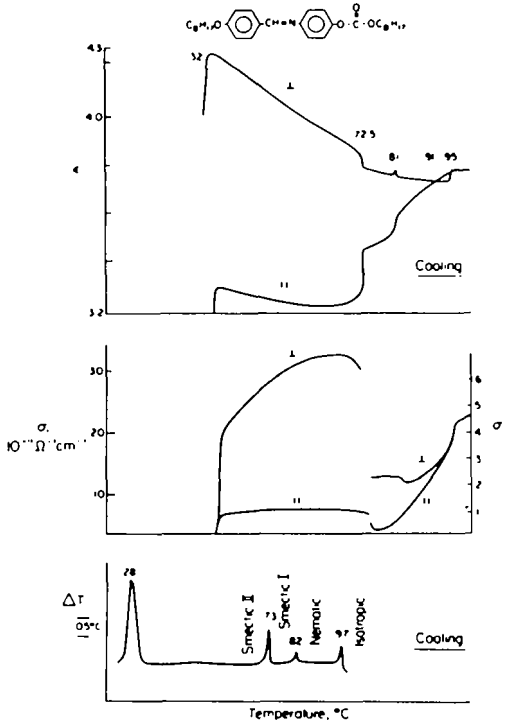

FIGURE 3 Dielectric and conductivity anisotropy upon cooling of N-(*p*-octyloxybenzylidene)-*p*'-octyloxycarbonyloxyaniline, with its corresponding DTA spectrum.

of the supercooled smectic II phase occurs at nearly the same temperature for both branches of the cooling curve as well as for the DTA sample (cf. lowermost plot), which has a completely different environment. This seems to be generally true for the various compounds we have studied, and may indicate that the crystallization temperature might depend strongly on the degree of order within the mesophase rather than upon some chance nucleation. It may be that the measured temperature of transition between a stable phase and a metastable phase of comparable order is more reproducible than if the relative order of the phase differs greatly, as in the case of supercooled isotropic liquids going to crystalline solids. Figure 4 illustrates the correspondence between the DTA and the observed dielectric behaviour upon heating. The DTA technique is capable of showing the melting of the crystalline solid at 60°C, which we are unable to observe since our sample cell must be filled with a liquid. The DTA spectrum obtained upon heating the crystalline solid is labeled "1st melting" in Figure 4. Upon cooling to the ploycrystalline solid (cooling curve in Figure 3) and then reheating, a "2nd melting" curve is obtained. This second melting DTA curve physically corresponds to our heating curves for anisotropy measurements.

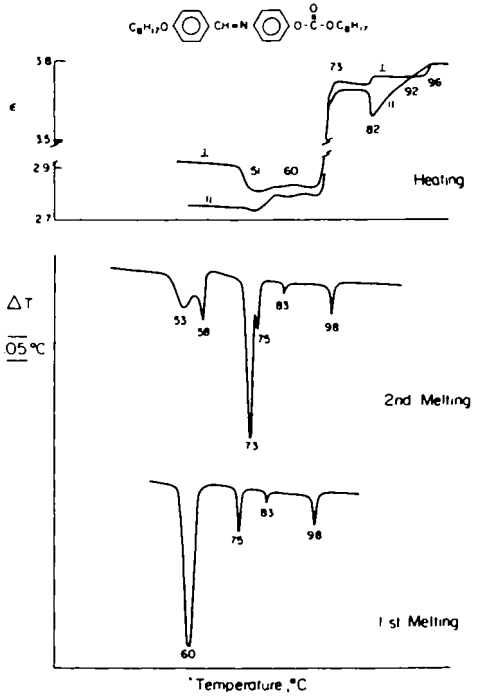

FIGURE 4 Dielectric anisotropy upon heating of N-(*p*-octyloxybenzylidene)-*p*'-octyloxycarbonyloxyaniline.

Notice that the permittivity heating curve and the DTA second melting curve reflect very similar thermal characteristics. Furthermore, the second melting is significantly different from the first. In the present case, the solid-to-smectic II transition has shifted upward 13C°, from 60°C to 73°C in the case of the second melting. Also two solid-solid transitions (or "premelting" transitions) now occur near 50°C and 60°C, and are observable both in the DTA and anisotropy data. The most striking feature of this compound is the reversal in sign of the dielectric anisotropy, within the nematic phase, from positive to negative at 91°C. There occurs no such reversal in the conductivity, although the magnitude of the conductivity anisotropy is increasing with decreasing temperature rather than decreasing as in MBBA. Furthermore, $\sigma_\perp$ is greater than $\sigma_\parallel$ throughout the nematic range; consequently, it is in the region of positive dielectric anisotropy that this material would satisfy the Helfrich criterion for dynamic scattering.

One might suspect that $\epsilon_\parallel$ is experiencing a dielectric loss at 10 kHz. Throughout the nematic phase, however, the temperature dependence of $\epsilon_\parallel$ remains unchanged from 10 Hz to 100 kHz. A dielectric loss definitely occurs in the smectic phases somewhere between 100 Hz and 1 kHz.

It is also observed that the anisotropies in the smectic phases, as measured, are not the same in the cooling curves as in the heating curves. The magnetic field is not influential in these phases, as evidenced by the invariability of the cell capacitance and conductance as the sample is rotated in the magnetic field once the smectic phases have formed. The magnetic field may, however, determine the preferential molecular direction within the smectic planes, upon cooling from the oriented nematic phase. When it is being heated from the crystalline solid, the crystalline phase dominates the smectic texture, which if formed heterogeneously throughout the sample, will appear quasi-isotropic and thus show a small anisotropy. As we have not been able to make microscopic observations of our samples in the magnetic fields, such interpretations must remain speculative.

We have also observed reversals in the sign of the conductivity anisotropy in the absence of any similar change in the dielectric anisotropy. An example is the Schiff base N-(*p*-octyloxycarbonyloxybenzylidene)-*p*'-octyloxyaniline. This compound is the analog to the former compound, with the *p*,*p*' substituents reversed. The material anisotropies are shown in Figure 5. Since this material exhibits a negative dielectric anisotropy throughout the nematic phase, whereas the conductivity anisotropy reverses sign at 90.8°C, one would expect the gradual disappearance of the electrically induced hydrodynamic instabilities of the Carr-Helfrich type as the nematic phase is cooled. We have observed this visually and present a more quantitive example in Figure 6 for the compound N-(*p*-pentyloxycarbonyloxybenzylidene)-*p*'-octyloxyaniline, which exhibits a sign reversal in $\Delta\sigma$ near 78°C. At temperatures above 78°C, the relative transmission of light through the sample is modulated at a frequency twice that of the applied

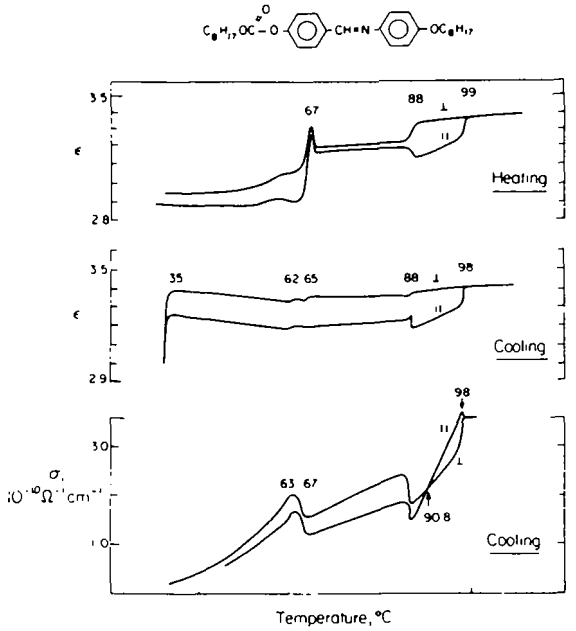

FIGURE 5 Dielectric and conductivity anisotropy of N-(*p*-octyloxycarbonnyloxybenzylidene)-*p*'-octyloxyaniline.

field frequency. One sees in Figure 6 that at 88°C for frequencies less than about 50 Hz, nearly 80 percent of the incident light is scattered out of the incident beam by the induced turbidity. Above 400 Hz the material fails to respond, and at intermediate frequencies a strong double-frequency modulation occurs (represented by the envelope of the modulated transmission in Figure 6). Below the conductivity anisotropy sign reversal, only a very slight change in relative transmission is observed. The relative transmission data correspond to a sample thickness of 12 μm with an applied potential of 100 V_{rms} swept in frequency from 0-500 Hz at a rate of 50 Hz/sec.

It is our observation that, in general, a positive conductivity anisotropy is associated with a nematic phase, whereas a negative conductivity anisotropy seems to be associated with smectic phases. Further, the kind of anisotropy seems to be independent of the particular dopant and liquid crystal employed, being mainly a feature of the particular mesophase present. We therefore conclude that the change in the sign of the conductivity anisotropy is a pretransitional effect. The negative conductivity in the smectic phase apparently arises from enhanced conductivity between the smectic planes which have formed uniformly oriented with respect to the magnetic field upon cooling from the

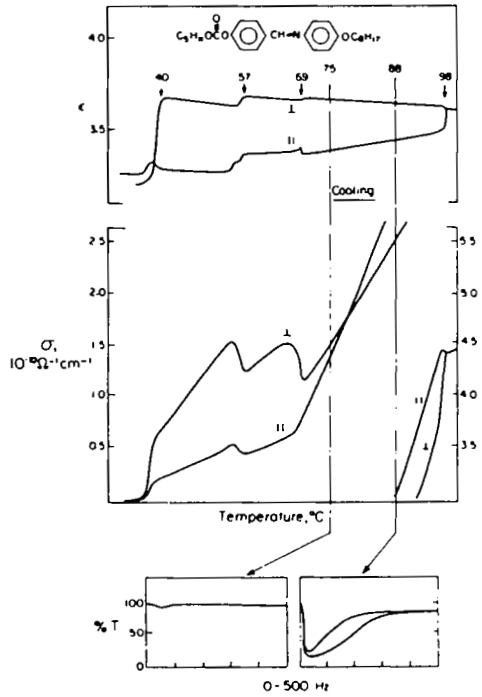

FIGURE 6 Relative transmission of N-(*p*-pentyloxycarbonyloxybenzylidene)-*p*'-octyloxyaniline above and below the conductivity reversal temperature upon applying 100V rms at the indicated frequencies.

oriented nematic phase. If the smectic A phase is formed, the smectic planes would be parallel to the electric field for the geometry used to measure $\sigma_{\parallel}$ (i.e., E perpendicular to H). For different smectic phases, the planes would be titled with respect to the electric field such that the molecular long axis remains parallel to the magnetic field. By maintaining the molecular long axis and the magnetic field parallel, one can envision the nematic transition, upon cooling from the oriented nematic phase, to simply require translation of molecular centers in the direction of the molecular long axis. In the pretransitional smectic local ordering, there would then occur some distribution of molecular centers at which the ionic mobility would be the same both parallel and perpendicular to the molecular axis and $\Delta\sigma$ would vanish. Figure 6 shows that the pretransitional local order can extend into the nematic phase by at least 9C°. In fact, the conductivity behavior illustrated by Figure 3 may suggest smectic local order throughout the entire nematic phase, even though this material exhibits a normal nematic appearance microscopically throughout the nematic range.

b. *Effect of Alkyl Chain Length:* We have studied the effect of alkyl chain length on two series of compounds:

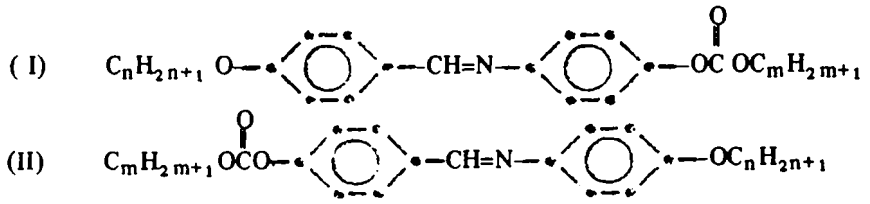

The indices n and m indicate the alkyl chain length on the alkoxy ($C_nH_{2n+1}O$–) substituent and carbonate ($-OCOC_mH_{2m+1}$) substituent, respectively. Figure 7 shows the cooling curves for the dielectric anisotrophy for series (I) where n+m has been kept constant to maintain a comparable molar volume for all compounds. We observed that the general shapes of the cooling curves are all rather similar. The greatest temperature dependence is in $\epsilon_\parallel$; notice that $\bar{\epsilon}$ at the clearing temperature is nearer $\epsilon_\perp$ than expected from the relation $\epsilon = \frac{1}{3}(2\epsilon_\perp + \epsilon_\parallel)$, whereas $\Delta\epsilon$ is negative. We think that $\epsilon_\parallel$ may be lower than expected.

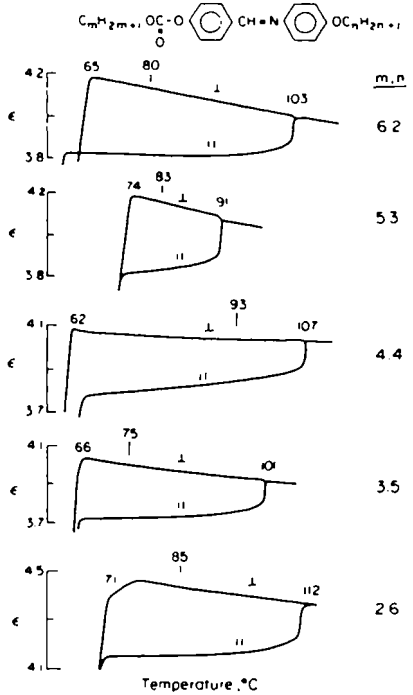

FIGURE 7 Dielectric anisotropy of a homologous series of carbonate alkoxy Schiff bases. The vertical bars represent the crystalline melting temperatures.

The anisotropy $\Delta\epsilon$ is the same, within experimental error, for the entire series when compared at the same reduced temperature, T/T_C. The analogous alkoxycarbonate series (II), n+m = 8, shows a quite different temperature dependence in the dielectric anisotropy, as is apparent in Figure 8. The anisotropy is now positive near the nematic-isotropic transition temperature and experiences a sign reversal at a temperature which increases with increasing m. Since the temperature dependence of $\epsilon_\parallel$ is nearly the same for all members of the series, the varying anisotropy is due primarily to the temperature dependence of $\epsilon_\parallel$. In fact, $\epsilon_\parallel$ becomes progressively smaller with increasing carbonate alkyl chain length m. In the case of a similar compound, (see Figure 9), $\epsilon_\parallel$ has become smaller than $\epsilon_\perp$ throughout the entire nematic phase. The conductivity anisotropy for both the (I) and (II) series is positive and varies smoothly with temperature throughout the nematic phase. As these materials were not intentionally doped, the observed conductivities are due to impurities present from their preparation. Owing to the high activation energy, typically 0.7 – 0.9 eV, of the conductivity, the impurity levels of dissociable species must be less than 10^{-6}:1 to result in a conductivity of $\sim 10^{-10}\ ^{-1}\,cm^{-1}$ at elevated tempe-

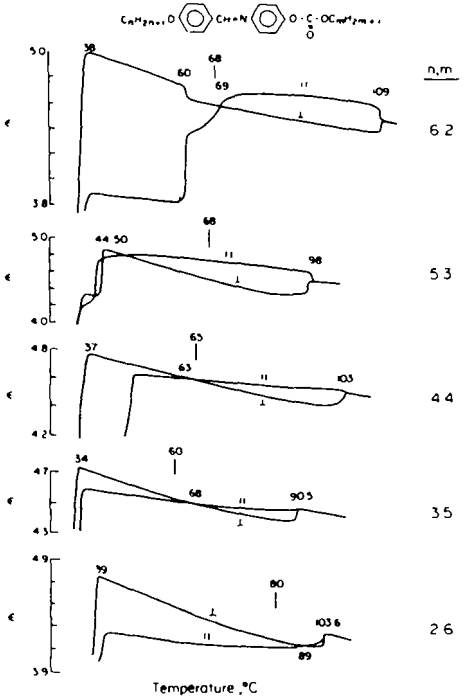

FIGURE 8 Dielectric anisotropy of a homologous series of alkoxy carbonate Schiff bases.

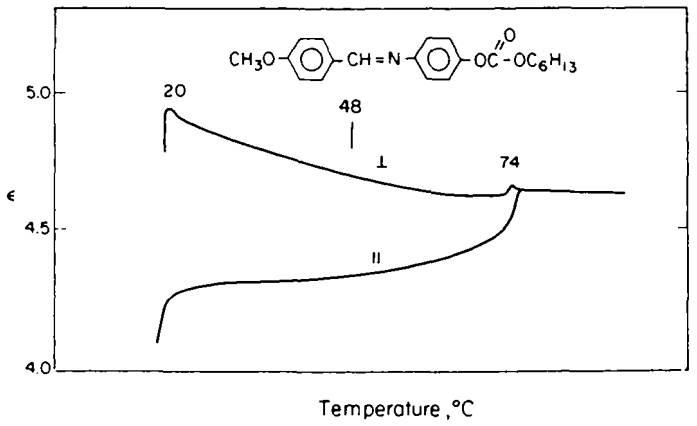

FIGURE 9 Dielectric anisotropy of N-(*p*-methoxybenzylidene)-*p*'-hexyloxycarbonyloxy-aniline.

ratures. The conductivity can be expected to increase by an order of magnitude with each 30°C of increased temperature.

c. *Dielectric Properties of Some p-Phenyl Benzoates:* We have also examined the dielectric anisotropies of some esters of the form:

(III) 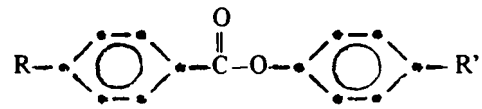

where R or R′ have been an alkyl ($-C_nH_{2n+1}$) or alkoxy ($C_nH_{2n+1}O-$) substituent. The chain length n simply corresponds to those compounds available to us which had the lowest clearing temperatures. The observed anisotropies for some representative coumpounds are shown in Figure 10. The anisotropy $\Delta\epsilon$ is most positive for the compound having paraffin end groups, R and R′. The introduction of polar alkoxy end groups results in a more negative anisotropy. The effect is greater for an alkoxy group in the R′ position. Consequently, when both R and R′ are alkoxy substituents, the anisotropy is most negative.

d. *Dielectric Anisotropy of p-Phenyl p-Benzoyloxybenzoates:* Besides the *p*-phenyl benzoates, we have also examined several double esters of the forms:

(IV) 

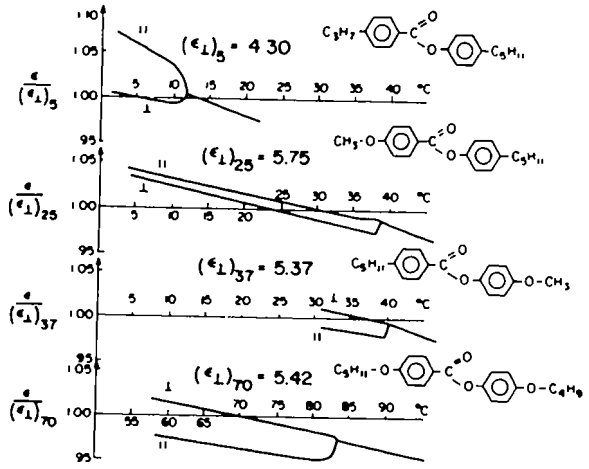

FIGURE 10 Dielectric anistropy of several phenyl benzoate derivatives.

and

(V) 

where, again, R and R′ are alkoxy, alkyl, or carbonate substituents. Our measurements on these compounds are not as extensive as those on I, II, and III, and so far these appears to be little variation among the materials. A representative compound is the chlorinated compound

(VI) 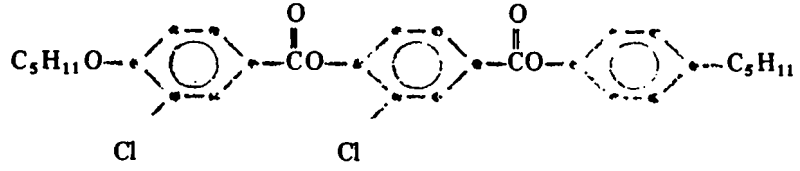

The dielectric anisotropy is shown in Figure 11. The dielectric anisotropy is negative throughout the nematic phase; however, there occurs a dielectric loss in $\epsilon_\parallel$ associated with the rotation about the molecular short axis.

An idealized example of a dielectric loss in $\epsilon_\parallel$ is expressed by Eq. 3:

$$\left.\begin{aligned} \frac{\epsilon' - \epsilon'_\infty}{\epsilon'_0 - \epsilon'_\infty} &= \sum_i \frac{1}{1+\omega^2\tau_i^2} \\ \frac{\epsilon''}{\epsilon'_0 \ldots \epsilon'_\infty} &= \sum_i \frac{i}{1+\omega^2\tau_i^2} \end{aligned}\right\} \qquad (3)$$

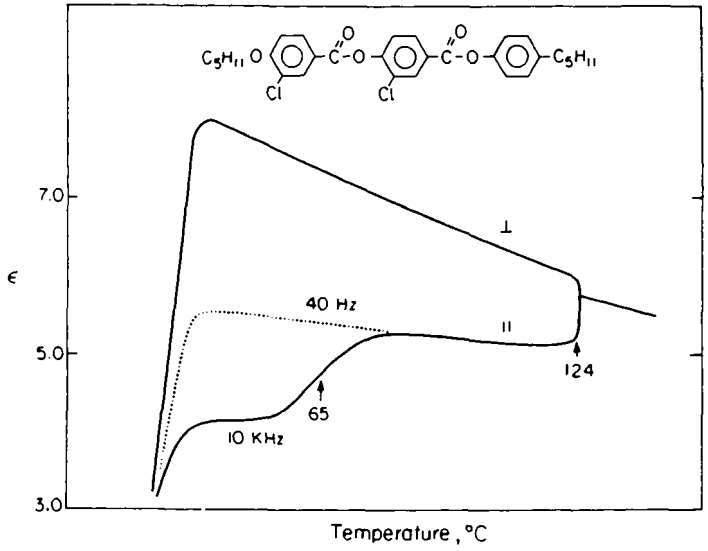

FIGURE 11 Low-frequency dielectric loss in $\epsilon_\parallel$ for a chlorinated phenyl-*p*-benzoyloxybenzoate.

where ω is the circular frequency of the applied electric field, and τ_i is the *characteristic relaxation time for the* i^{th} *relaxation process.*

A schematic representation of the frequency dependence of the capacitive component of the permittivity, ϵ', and the resitive component of the permittivity, ϵ'', is illustrated for several temperatures in Figure 12 which also defines a temperature-dependent relaxation frequency $\omega_{1/2}$. We assume a single relaxation process with a characteristic relaxation time, τ, related to the Debye relaxation time, τ_0, via a retardation factor $\tau = \tau_0[(kT/W)e^{W/kT}]$ (in the manner of Maier and Saupe).[7] The activation energy W is obtained from a log $(1/\omega_{1/2})$ *vs* 1/T plot as in Figure 13. Knowledge of W permits the calculation of $\epsilon(\omega,T)$; good agreement between the calculated and observed dielectric behavior of $\epsilon\parallel$ would then support the original assumption of a single relaxation process. This same analysis was made by M. Schadt[8] in his study of three Schiff base nitriles which possess an activation energy of about 0.7 eV.

Figure 13 shows the temperature dependence of the relaxation frequency, $\omega_{1/2}$, for a proprietary room-temperature nematic mixture of phenyl-*p*'-benzoyloxybenzoates and corresponds to an activation energy of 0.93 eV. The calculated $\epsilon(T,\omega)$ is compared with the experimental value in Figure 14 for a frequency of 10 kHz. Such behavior is not limited to mixtures, of course; an example is compound VII, which exhibits the 10 kHz dielectric anisotropy inversion at 55°C as depicted in Figure 15.

(VII) 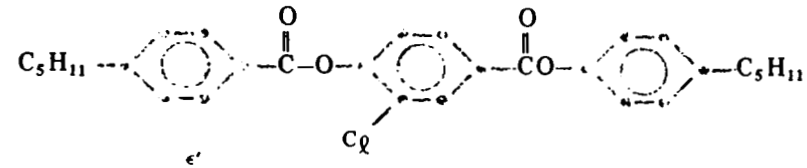

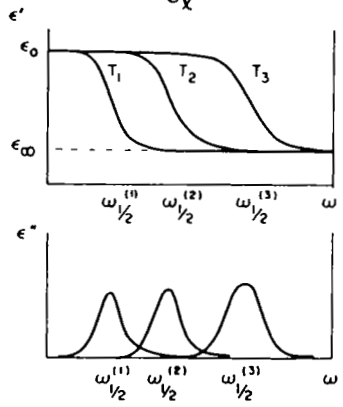

FIGURE 12 An idealized example of dielectric behavior for a single relaxation process.

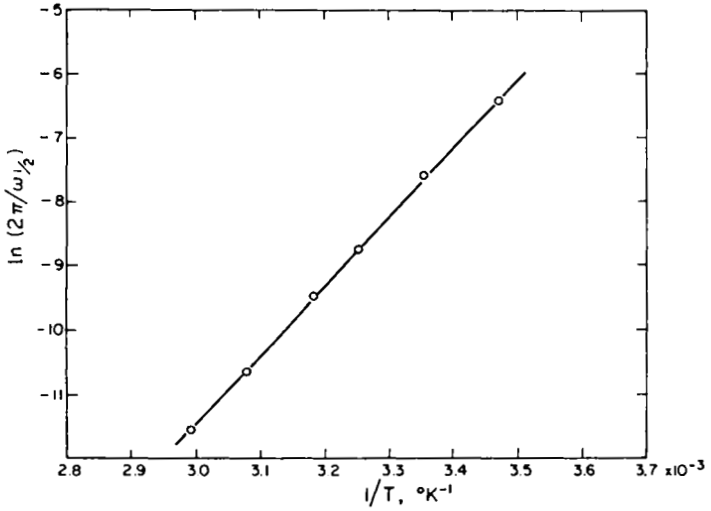

FIGURE 13 Activation energy for the dielectric loss in $\epsilon_{\parallel}$ for a room-temperature nematic mixture of phenyl-*p*-benzoyloxybenzoates.

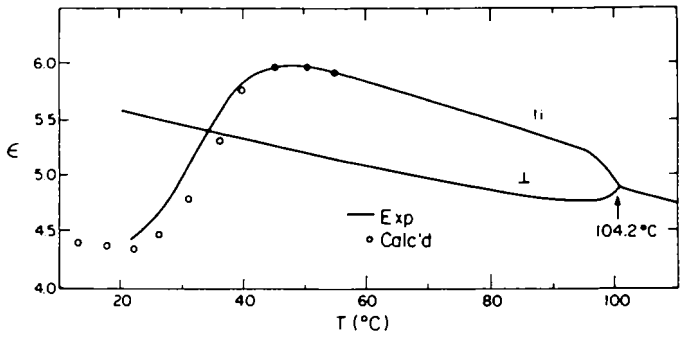

FIGURE 14 Calculated temperature dependence of $\epsilon_{\parallel}$ from the measured activation energy, assuming a single relaxation process.

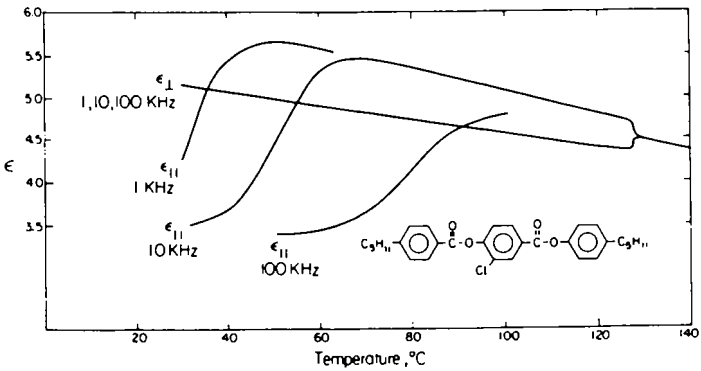

FIGURE 15 Low-frequency dielectric loss in $\epsilon_{\parallel}$ exhibited by 4-*n*-pentylphenyl-4-(4-pentylbenzoyloxy)-3-chlorobenzoate.

Unlike the frequency-independent inversion described in Section 4a, the inversion in this case is simply the result of the dielectric loss in $\epsilon_{\parallel}$ occurring at unusually low frequencies.† This unusually low relaxation frequency of the double esters is, presumably, due to the greater molecular length of the double esters compared to the Schiff bases, as well as the increased intermolecular attraction resulting from the added phenyl ring. Such low frequencies obviously do not represent free molecular reorientation but, rather, the long-range cooperative motion of the molecular long axis. Figures 14 and 15 also illustrate the broaden-

†This behaviour has also been observed for similar compounds by Dr. W. H. DeJeu, Philips Research Laboratories, Eindhoven, Netherlands, and was reported by him at the Fourth International Liquid Crystal Conference, Kent State University, 1972. See also, DeJeu et al., Phys. Lett., *39A*, 355 (1972).

ing of the nematic isotropic transition that occurs in mixtures, compared to the transition for single-component fluids.

SUMMARY

The selection of liquid crystalline materials for device applications involving electric fields will undoubtedly require optimizing their dielectric and conductivity anisotropies. We have shown that these anisotropies are dependent upon molecular structure and temperature in varying ways. Even within the nematic phase, we have observed sign reversals in the dielectric and conductivity anisotropies with changing temperature. The temperature at which the anisotropy vanishes is not frequency dependent from 10 to 10^5 Hz and is not accompanied by a thermal transition. The sign reversal of the dielectric anisotropy is not necessarily accompanied by a similar reversal in the conductivity anisotropy as each reversal apparently arises from different causes. A reversal in the dielectric anisotropy also occurs when $\epsilon_\parallel$ experiences a dielectric loss providing the zero frequency anisotropy is positive. In this latter case, the temperature at which the reversal occurs will depend on the frequency of the electric field.

Characterization of the dielectric behavior in smectic phases has not yet been possible, since we lack sufficient knowledge of the smectic plane orientations. However, we have seen a means to influence smectic plane orientation by cooling from the nematic phase, which is aligned by an external magnetic field. Furthermore, since dielectric measurements are easy to make, they provide a simple means to observe transition temperatures among the mesophases. We hope that correlation of dielectric and conductivity phenomena with thermal data and molecular structure may eventually provide a tool for characterizing liquid crystalline phases as well as providing a measure of important material parameters necessary for device applications.

Acknowledments

We are grateful to T. R. Criswell and J. P. Van Meter for the preparation and purification of the liquid crystal materials used in this study, and to S. E. B. Petrie for providing DTA information. We also thank B. H. Klanderman for stimulating discussions and helpful suggestions.

References

1. Carr, E. F., *Mol. Cryst. Liquid Cryst.*, 7, 253 (1969).
2. Helfrich, W., *J. Chem. Phys.*, 51, 4092 (1969).
3. Pincus, P., *C. R. Acad. Sci. Paris.*, 267B, 1230 (1968).
4. Frank, F. C., *Disc. Faraday Soc.*, 25, 19 (1938).

5. Heilmeier, G., Sanoni, L. A., and Barton, L. A., *Proc. IEEE*, **56**, 1162 (1968).
6. Schwerdtfeger, C. F., et al., *Mol Cryst. Liquid Cryst.*, **12**, 335 (1971).
7. Maier, G., and Saupe, A., *Mol. Cryst. Liquid Cryst.*, **1**, 515 (1966).
8. Schadt, M., *J. Chem. Phys.*, **56**, 1494 (1972).
9. DeJeu, W. H., Gerritsma, C. J., VanZanten, P., Gossens, W. J. A., *Phys. Lett.*, **39A**, 355 (1972).